A multicentre-bonded $[Zn^I]_8$ cluster with cubic aromaticity

Ping Cui[1,*], Han-Shi Hu[2,*], Bin Zhao[1], Jeffery T. Miller[3], Peng Cheng[1] & Jun Li[2]

Polynuclear zinc clusters $[Zn_x]$ ($x > 2$) with multicentred Zn–Zn bonds and $+1$ oxidation state zinc (that is, zinc(I) or Zn^I) are to our knowledge unknown in chemistry. Here we report the polyzinc compounds with an unusual cubic $[Zn^I_8(HL)_4(L)_8]^{12-}$ (L = tetrazole dianion) cluster core, composed of zinc(I) ions and short Zn–Zn bonds (2.2713(19) Å). The $[Zn^I_8]$-bearing compounds possess surprisingly high stability in air and solution. Quantum chemical studies reveal that the eight Zn $4s^1$ electrons in the $[Zn^I_8]$ cluster fully occupy four bonding molecular orbitals and leave four antibonding ones entirely empty, leading to an extensive electron delocalization over the cube and significant stabilization. The bonding pattern of the cube represents a class of aromatic system that we refer to as cubic aromaticity, which follows a $6n + 2$ electron counting rule. Our finding extends the aromaticity concept to cubic metallic systems, and enriches Zn–Zn bonding chemistry.

[1] Department of Chemistry, Key Laboratory of Advanced Energy Material Chemistry of the Ministry of Education, Tianjin Key Laboratory of Metal and Molecule Based Material Chemistry, and Collaborative Innovation Center of Chemical Science and Engineering (Tianjin), Nankai University, Tianjin 300071, China. [2] Department of Chemistry and Laboratory of Organic Optoelectronics and Molecular Engineering of the Ministry of Education, Tsinghua University, Beijing 100084, China. [3] Chemical Sciences and Engineering Division, Argonne National Laboratory, Argonne, Illinois 60439, USA. * These authors contributed equally to this work. Correspondence and requests for materials should be addressed to B.Z. (email: zhaobin@nankai.edu.cn) or to J.L. (email: junli@tsinghua.edu.cn).

Chemical bonding is the cornerstone of the whole chemistry edifice[1,2]. Among the various bonding types, metal–metal (M–M) bonding has been one of the most important themes in inorganic chemistry since Cotton et al.[3] proposed the concept of M–M quadruple bonding in the $[Re_2Cl_8]^{2-}$ ion in 1964. Especially noteworthy in this field are the findings of novel structures and applications of uncommon low oxidation state (LOS) M–M bonded compounds stabilized by sterically bulky ligands. Great progress has been recently witnessed by successful syntheses of compounds with single M^I-M^I bonds (for example, M = Zn (ref. 4), In (ref. 5), Mg (ref. 6), Co (ref. 7), Cd (ref. 8)) and those with quintuple M–M bonds between Cr^I (ref. 9) or Mo^I (ref. 10). Among those, the landmark discovery of decamethyldizincocene $[Cp^*ZnZnCp^*]$ ($Cp^* = C_5Me_5$) with a covalent Zn^I-Zn^I bond by Carmona and coworkers in 2004 initiated the epoch of Zn–Zn bonding chemistry[11–23]. However, these studies focus on the $[Zn_2]^{2+}$ dimeric species that are not sufficiently stable in air[11]. So far, no polyzinc cluster $[Zn_x]^{x+}$ (x > 2) with multicentred Zn^I-Zn^I bonds are known.

Here we report the synthesis, characterization and theoretical analysis of two Zn^I compounds with a rare cubic $[Zn^I_8(HL)_4(L)_8]^{12-}$ (L = tetrazole dianion) cluster containing multicentred Zn–Zn bonds. These Zn^I_8-bearing compounds are surprisingly stable in solutions and in air at temperature far above ambient temperature. Quantum chemical studies reveal extensive electron delocalization over the Zn^I_8 cube. Our finding extends the aromaticity concept from the all-metal aromaticity[24–30] and spherical aromaticity obeying $2(n+1)^2$ rule[31] to cubic metal systems.

Results

Syntheses. To form LOS Zn–Zn-bonded compounds, we designed a series of reactions for the in situ reduction of Zn^{II} compounds under a solvothermal condition. The same approach was used previously for in situ reduction of Cu^{II} and Fe^{III} to yield LOS ions[32]. Here we report the syntheses of two compounds, $Na_{2.6}K_{1.4}\{[Na(DMF)]_8[Zn_8(HL)_4(L)_8]\} \cdot 8H_2O \cdot 2H_2L \cdot DMF$ (**1**) and $Na_3K_{2.33}\{K_4[Na(DMF)_3]_{1.33}[Zn^{II}Br]_{1.33}[Zn_8(HL)_4(L)_8]\} \cdot 2H_2O \cdot 2H_2L \cdot 4DMF$ (**2**) (DMF = N,N'-dimethylformamide), by in situ reactions of $K[C(CN)_3]$, NaN_3 and Zn^{II} salts under solvothermal conditions, with the yield of ~26 and ~15%, respectively. The crystals of **1** can also be produced by using ZnO or other organonitriles, such as 7,7,8,8-tetracyanoquinodimethane, biphenyl-4,4-dicarbonitrile, 1,1,3,3-tetrakis-cyanopropane and so on, although the yields are much lower and the qualities of the crystals are relatively poor (Supplementary Table 1).

Analyses of stability. Both **1** and **2** are stable in air, as revealed by powder X-ray diffraction of the samples exposed to air for at least half a year (Supplementary Figs 1 and 2) and thermogravimetry analyses (Supplementary Fig. 3). These two kinds of compounds are insoluble in common organic solvents. However, **1** can easily dissolve in water and recrystallize on adding DMF into water, as is supported by crystal structure analyses of the recrystallized samples. It follows that the $[Zn_8(HL)_4(L)_8]^{12-}$ cluster can stably exist in water, which is further confirmed by the high-resolution electrospray ionization mass spectrometry (ESI-MS) of **1** in water. Series of zinc isotope peaks centred at $m/z = 738.8141$ are clearly observed (Supplementary Figs 4 and 5), and the simulated MS patterns of the molecular fragment $\{[Zn_8(HL)_4(L)_8][Na_4(H_2O)_2] + 6H\}^{2-}$ (calcd. 738.8128) containing $[Zn_8(HL)_4(L)_8]^{12-}$ cluster match well with the corresponding experimental isotope peaks. This high stability of the $[Zn_8(HL)_4(L)_8]^{12-}$ cluster is in striking contrast with the

existing $[Zn_2]^{2+}$ compounds, which survived only in low temperature and were so air sensitive as to burn out spontaneously[4].

Structural analyses. The molecular structures of **1** and **2** were determined by single-crystal X-ray diffraction, and their non-hydrogen atoms were also identified by X-ray photoelectron spectroscopy (XPS) analyses (Supplementary Fig. 6). In addition, small molecules or cations within the pores of **1** and **2**, such as DMF, Na^+, K^+, H_2L and H_2O, were characterized by ^1H and ^{13}C nuclear magnetic resonance (NMR), ion chromatography (Supplementary Fig. 7), infrared spectra (IR), elemental analyses and inductively coupled plasma (ICP). While crystallized in different space groups of $I4/m$ for **1** and P-$43m$ for **2**, they possess a unique tetragonally distorted Zn^I_8 cubic cluster with direct multicentred Zn–Zn bonding, and the Zn^I_8 core is supported by twelve tetrazole rings, forming $[Zn^I_8(HL)_4(L)_8]^{12-}$ motifs. In addition to the Zn–Zn bonds, the adjacent two Zn^I ions are further connected by two N atoms from the tetrazole ring ligands, which orient along the corresponding twelve edges of the Zn^I_8 cube. Thus, each Zn^I ion coordinates to three N atoms of the tetrazole ligands and three neighbouring Zn^I ions in the cube. Different from all previously reported $[Zn_2]^{2+}$ species[11], where various bulky ligands, for example, C_5Me_5, $[\{(2,6-i-Pr_2C_6H_3)N(Me)C\}_2CH]$, and $[2,6-(2,6-i-Pr_2C_6H_3)C_6H_3]$, were utilized to protect the Zn^I-Zn^I bond, compounds **1** and **2** provide the first example of stable Zn^I-Zn^I bonds supported only by small tetrazole ligands.

In these compounds, eight Zn^I ions act as the vertices of the distorted cube, forming Zn^I_8 core with D_{4h} symmetry in **1** and D_{2d} symmetry in **2**. There are twelve Zn^I-Zn^I bonds in **1** (Fig. 1), with four Zn^I-Zn^I bond lengths of 2.292(2) Å and eight Zn^I-Zn^I ones of 2.4810(18) Å. All these twelve Zn^I-Zn^I bond lengths are smaller than the sum of Pauling's single-bond metallic radii (2.50 Å) (ref. 2), suggesting the existence of direct Zn–Zn bonds. In the Zn^I_8 cube of **2** (Fig. 2), due to the lower local symmetry, twelve Zn^I-Zn^I bonds divide into three groups, corresponding to three types of bond lengths of 2.394(2), 2.766(2) and 2.2713(19)

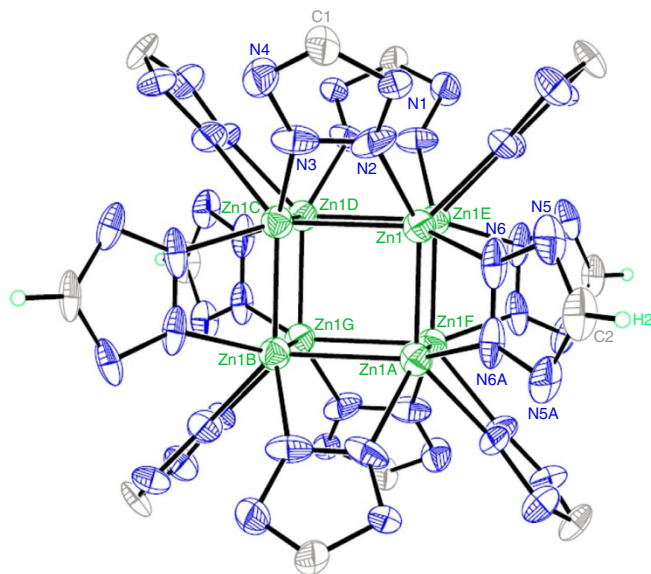**Figure 1 | Structure of cluster $\{Zn_8(HL)_4(L)_8\}^{12-}$ in 1.** Selected bond distances (Å): Zn1-Zn1A (Zn1B-Zn1C, Zn1D-Zn1G, Zn1E-Zn1F) = 2.292(2), Zn1-Zn1C (Zn1-Zn1E, Zn1A-Zn1B, Zn1A-Zn1F, Zn1B-Zn1G, Zn1C-Zn1D, Zn1D-Zn1E, Zn1F-Zn1G) = 2.4810(18). Thermal ellipsoids are set at the 25% probability level.
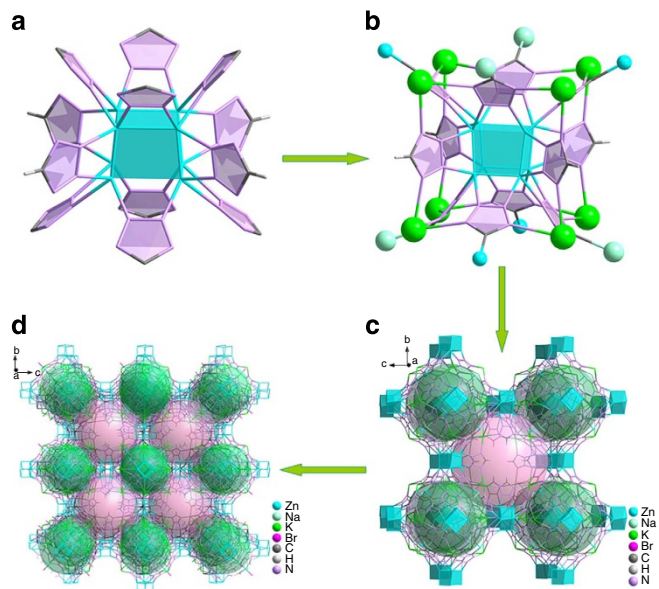
Figure 2 | Three-dimensional (3D) framework structure of 2. (**a**) The $\{Zn_8(HL)_4(L)_8\}^{12-}$ cluster and Zn^I_8 cube structure (blue cube) in **2**. (**b**) The connections among the cluster and Na^+, K^+, Zn^{II}. (**c**) Eight clusters as nearest neighbours around each cluster. (**d**) The 3D framework with the alternatively arranged closed cages (green) and open cages (pink).

Å, where the latter is slightly shorter than the shortest Zn–Zn bonds (2.295 Å) in $Zn_2(\eta^5\text{-}C_5Me_4Et)_2$ (ref. 14), and the four Zn^I–Zn^I bonds of 2.766(2) Å are weaker.

In **1**, each $[Zn^I_8(HL)_4(L)_8]^{12-}$ cluster is linked to eight such clusters as its nearest neighbours by sixteen Na^+ ions, forming a three-dimensional metal-organic framework (Supplementary Figs 8 and 9). In **2**, the C and N atoms in the $[Zn^I_8(HL)_4(L)_8]^{12-}$ cluster coordinate to external Zn^{II}, Na^+ and K^+ ions, generating two types of cages (Supplementary Fig. 10). The small closed cages and large open cages are alternately arranged, giving a fascinating three-dimensional framework (Fig. 2). Each closed cage consists of six $[Zn^I_8(HL)_4(L)_8]^{12-}$ clusters, four Zn^{II}, four Na^+ and twelve K^+, while each open cage is constructed by twelve $[Zn^I_8(HL)_4(L)_8]^{12-}$ clusters, four Zn^{II}, four Na^+ and twenty-four K^+. These different types of ions connected with the $[Zn^I_8(HL)_4(L)_8]^{12-}$ cluster significantly influence the ultraviolet–visible and luminescence spectra of **1** and **2** (Supplementary Fig. 11).

Spectrocopic and theoretical studies. The existence of Zn^I–Zn^I bonds in **1** and **2** is supported by both experimental and theoretical evidences. From the measured Raman spectra of **1** and **2** (Supplementary Fig. 12), several low-frequency vibration peaks involving the contribution of Zn–Zn stretching modes are observed between 100 and 400 cm^{-1} (refs 18–20), but a clear-cut assignment is difficult due to significant Zn–Zn and Zn–L modes mixing. Geometry optimizations, bond order and electron localization function (ELF) calculations using density functional theory methods also confirm direct Zn–Zn bond. We find that the different Zn–Zn distances in **1** and **2** are related to the varied donation ability of the tetrazole ligand with different outside cations, indicating the tetrazole ligands also play a role in stabilizing the Zn^I_8 clusters. The theoretically predicted Zn–Zn distances are 2.43, 2.46 Å in **1**, and 2.32, 2.42 and 2.81 Å in **2** (Supplementary Table 2), which agree well with their corresponding experimental values of 2.29, 2.48 Å in **1** and 2.27, 2.39 and 2.77 Å in **2**. The Mayer bond orders of Zn–Zn bonds are
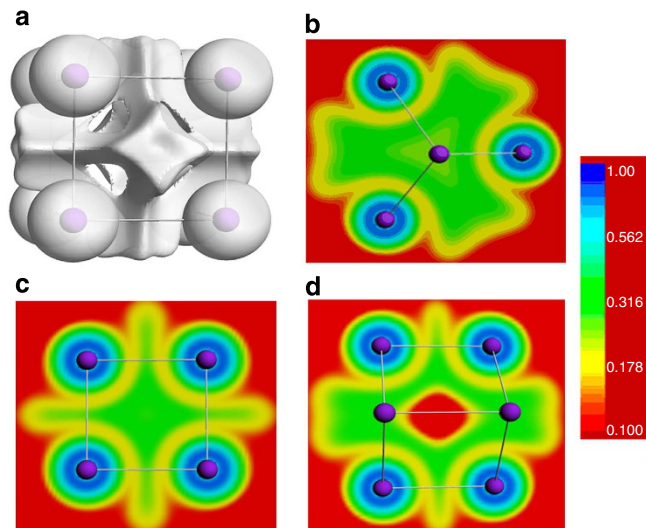

Figure 3 | ELFs for Zn_8^{8+}. (**a**) The isosurface of the cube. (**b**) The triangular surface. (**c**) The square surface. (**d**) The diagonal rectangular surface.

calculated as 0.32 and 0.35 in **1**, as well as 0.48, 0.34, and 0.14 in **2**, consistent with each Zn connecting to three adjacent Zn in the cube. The ELF contours also show significant electron-pair density along the Zn–Zn bond, supporting direct Zn–Zn bonding in the clusters (Fig. 3).

As Zn^I is usually much less stable than Zn^{II} in chemistry, it is remarkable that all the zinc atoms in the Zn_8 core of **1** and **2** exist in a +1 oxidation state. The XPS data reveal that the binding energy of Zn ions appears at 1019.5 eV for **1** and 1020.1 eV for **2** (Supplementary Fig. 6), which is markedly smaller than the reported Zn $2p_{3/2}$ binding energy (1021.8 eV) of Zn^{II} ions[33]. As LOS always has smaller binding energy than its higher one, the large deviation to our experimental values from those of Zn^{II} ions suggests the presence of LOS Zn ions in **1** and **2**. By comparison with **1**, the Zn^{II} ions coordinated to Br atoms in **2** cause the broadening and blue-shift of the XPS peaks, thus accounting for their difference. We also carried out density functional theory calculations on the model clusters $[Na_8Zn_8(HL)_4(NaL)_8]^{n+}$ by assuming Zn^I ($n = 4$) or Zn^{II} ($n = 12$). The geometry optimized for the $[Zn^I_8]$ cluster agrees well with the experimental crystal structure, whereas that of $[Zn^{II}_8]$ will lead to extremely long Zn…Zn distance and eventually the collapse of $[Zn^{II}_8]$ cluster, providing additional credence for Zn^I in **1** and **2**.

X-ray absorption near-edge structures. We further performed X-ray absorption near-edge structure (XANES) analyses of four samples, including **1** and **2** together with $Zn(NO_3)_2 \cdot 6H_2O$ and Zn foil as standard control groups (Fig. 4). Although no previous XANES data of Zn^I ions are reported, there exists a linear correlation between the Zn K-edge energies of these samples and their formal oxidation states. Our XANES data show that the Zn K-edge energies in **1** and **2** exactly correspond to the +1 oxidation state, thus providing an unequivocal evidence for the existence of Zn^I ions in these compounds, originated from the reduction of Zn^{II} ions caused by the cleavage of C–C bonds.

Discussion

To elucidate the bonding of the Zn^I_8 cube and the special thermal stability of $[Zn^I_8(HL)_4(L)_8]^{12-}$ motifs in **1** and **2**, we have further investigated the Zn–Zn bonding properties and electronic structures of the $[Zn^I_8]$ systems using selected O_h, D_{4h} and D_{2d} model clusters. Our results show that the clusters have closed-
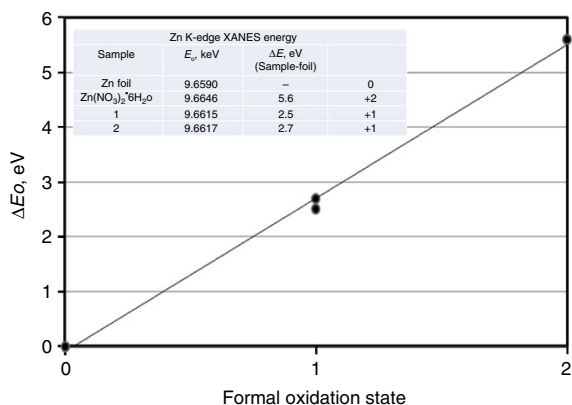
Figure 4 | The change of Zn K-edge energy versus oxidation state. The Zn foil edge energy (9.6590 keV) is selected as the reference energy, that is, $\Delta E_o = 0$. Inset: the Zn K-edge XANES energy.
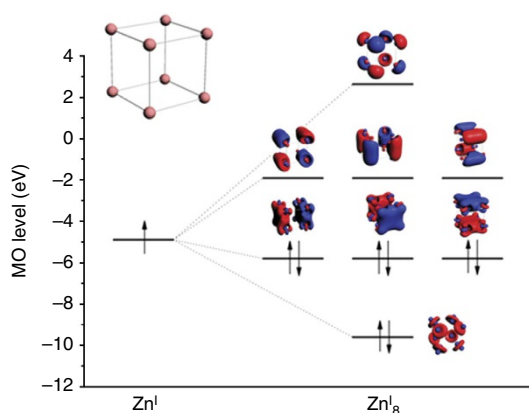

Figure 5 | The bonding pattern in Zn^I_8 with cubic aromaticity. Levels of Zn^I_8 are shifted relative to Zn^I.

shell electron configuration (Fig. 5), consistent with the EPR-silence and diamagnetic feature of the samples (Supplementary Figs 13 and 14). Inasmuch as Zn^I ion only possesses one $4s$ electron, eight delocalized molecular orbitals (MOs) of the Zn^I_8 cube are formed through overlap of the $4s$ orbitals, with slight mixing from the Zn $4p$ and Zn $3d$ orbitals. Among them, four bonding orbitals with a_{1g} and t_{1u} symmetry are fully occupied, giving a ground-state electronic configuration of $(a_{1g})^2(t_{1u})^6$, whereas four antibonding orbitals with t_{2g} and a_{2u} symmetry are completely empty. The bonding pattern of the eight MOs is comparable to those of Au_3^+ and benzene molecules that have the famous planar σ- and π-aromaticity[34] and obey Hückel's $4n + 2$ rule (Supplementary Fig. 15). This bonding pattern represents a rare type of aromaticity, which we refer to as cubic aromaticity. Such systems follow a $6n + 2$ electron counting rule or approximately the $2(n + 1)^2$ rule[29], which might help to search for heteroatomic cubic clusters with apt number of electrons.

This special cubic aromaticity arises from the electron delocalization over the entire Zn^I_8 cube. The calculated nucleus-independent chemical shift indices at the cubic-, face-, bond-centre display considerable negative values, which are comparable to those in benzene, also confirming the special aromaticity of the Zn^I_8 cube (Supplementary Table 3). Through theoretical analyses of the Zn^I_8 cube using analytic Hückel MO model and Kohn–Sham MOs, the estimated resonance energy ($4.00\ \beta_{ZnZn}$) appears to be comparable with that of benzene ($2.00\ \beta_{CC}$), far larger than $1.00\ \beta_{ZnZn}$ in reported Zn^I_2 compounds with Zn–Zn bonds,

where β is the resonance integral. Furthermore, the additional multi-centre bonding among the eight Zn atoms provides extra stabilization than the two-centre two-electron bonding in Zn_2 compounds. As a result, the cubic aromaticity, additional Zn $4p$ orbital interactions, and the strong metal-ligand interactions are responsible for the robustness of the $[Zn^I_8]$ core and the unique stability of the octanuclear Zn^I compounds.

Our finding of the stable $[Zn^I_8]$ motif to form self-assembled materials may have practical applications. Particularly, as these materials with specially stabilized Zn^I and the high energy density tetrazole rings[35] can undergo explosive combustion above 300 °C, they might find applications as propellants and high temperature explosives. The stable $[Zn^I_8]$ core with electron delocalization might be used to construct robust non-linear optical materials. Insofar as the special stability of the Zn^I_8 cube, we anticipate that the cubic aromaticity via s-, p-, d-, f-type atomic orbital overlap might also exist in other cubic metal cluster materials.

Methods

Synthesis of 1. Compound **1** can be obtained by the following five methods A–E, among which method A has the highest yield. Caution: owing to the explosive potential of NaN_3 and tetrazole-based compounds, only a small amount of material should be used and handled with care!

Method A. The mixture of $Zn(ClO_4)_2 \cdot 6H_2O$ (74.5 mg, 0.2 mmol), NaN_3 (65 mg, 1.0 mmol), NH_4F (11.1 mg, 0.3 mmol) and $K[C(CN)_3]$ (12.9 mg, 0.1 mmol) in DMF (6 ml) was sealed in a 25-ml Teflon-lined stainless steel autoclave and heated at 155 °C for 4 days and then cooled to room temperature at the rate of 1 °C per hour. Finally, colourless octahedral crystals of **1** were obtained directly, then washed with DMF and dried in air. Yield: 15.5 mg, 26% based on $K[C(CN)_3]$ (0.1 mmol). ICP analysis: Zn/Na/K molar ratio of 1:1.5:0.18. Anal. Calcd. (%) for $C_{41}H_{87}N_{65}O_{17}$-$K_{1.4}Na_{10.6}Zn_8$: C, 19.06; H, 3.39; N, 35.23. Found: C, 19.45; H, 4.12; N, 35.76. Selected IR (KBr, cm^{-1}): 3,426(vs), 2,934(w), 1,659(vs), 1,434(s), 1,390(s), 1,148(s), 1,106(m), 1,064(s), 950 (s), 771(w). High-resolution ESI-MS for **1** in H_2O/CH_3OH was performed and analysed with the anion mode. ^1H NMR (400 MHz; D_2O) δ 7.70 (1H), 2.59 (3H), 2.58 (3H); ^{13}C NMR (400 MHz; D_2O) δ 165.9, 164.8, 67.9, 36.5 31.2. As is usual, the absence of some H signals in tetrazole ^1H NMR spectra is due to the fast proton exchange.

Remarkably, the colourless polyhedral crystals (**1a**) were isolated after recrystallization of **1** from a H_2O/DMF mixture at room temperature, which were determined by single-crystal structure analysis. This result indicates that the $[Zn_8(HL)_4(L)_8]^{12-}$ cluster remains intact because Zn^I ions in water is very unstable and easily disproportionates into Zn(0) and Zn^{II}. **1a** would not be obtained by recrystallization if $[Zn_8(HL)_4(L)_8]^{12-}$ cluster had undergone the disproportionation reaction to decompose. Unfortunately, effort of exchanging free Na^+ and K^+ in **1** by other cations such as NH_4^+, $[N(CH_3)_4]^+$, and $[N(C_2H_5)_4]^+$ was not successful.

Method B. A mixture of ZnO (24.4 mg, 0.3 mmol), NaN_3 (19.5 mg, 0.3 mmol) and $K[C(CN)_3]$ (12.9 mg, 0.1 mmol) in DMF (6 ml) was sealed in a 25-ml Teflon-lined stainless steel autoclave and heated at 160 °C for 4 days and then cooled to room temperature at a rate of 1 °C per hour to form colourless octahedral crystals (**1b**), but with low yield.

Method C. A mixture of $ZnBr_2$ (45.0 mg, 0.2 mmol), NaN_3 (39 mg, 0.6 mmol) and 1,1,3,3-tetrakis-cyanopropane (14.4 mg, 0.1 mmol) in DMF (6 ml) was sealed in a 25-ml Teflon-lined stainless steel autoclave and heated at 160 °C for 4 days and then cooled to room temperature at the rate of 1 °C per hour. Finally, colourless square-pyramidal crystals (**1c**) were obtained directly, but with poor quality and low yield.

Method D. A mixture of $ZnBr_2$ (45.0 mg, 0.2 mmol), NaN_3 (39 mg, 0.6 mmol) and 7,7,8,8-tetracyanoquinodimethane (20.4 mg, 0.1 mmol) in DMF (6 ml) was sealed in a 25-ml Teflon-lined stainless steel autoclave and heated at 160 °C for 4 days and then slowly cooled to room temperature at the rate of 1 °C per hour. Finally, colourless square-pyramidal crystals (**1d**) were obtained directly, but with poor quality and low yield.

Method E. A mixture of $ZnBr_2$ (67.6 mg, 0.3 mmol), NaN_3 (39 mg, 0.6 mmol) and biphenyl-4,4′-dicarbonitrile (10.2 mg, 0.05 mmol) in DMF (6 ml) was sealed in a 25-ml Teflon-lined stainless steel autoclave and heated at 160 °C for 4 days and then slowly cooled to room temperature at the rate of 1 °C per hour. Finally, colourless square-pyramidal crystals (**1e**) were obtained directly, but with poor quality and low yield as well.

Synthesis of 2. The mixture of $ZnBr_2$ (135.2 mg, 0.6 mmol), NaN_3 (39 mg, 0.6 mmol) and $K[C(CN)_3]$ (25.8 mg, 0.2 mmol) in DMF (6 ml) was sealed in a 25-ml Teflon-lined stainless steel autoclave and heated at 170 °C for 4 days and then slowly cooled to room temperature at the rate of 1 °C per hour. Finally, pale-yellow cubic crystals of **2** were obtained directly and were then washed with ethanol and dried in air. Yield: 22.5 mg, 15% based on $K[C(CN)_3]$ (0.2 mmol). ICP analysis: Zn/Na/K molar ratio of 1:0.44:0.6. Anal. Calcd. (%) for $C_{38}H_{68}N_{64}O_{10}Br_{1.33}Na_{4.33}K_{6.33}Zn_{9.33}$: C, 17.26; H, 2.59; N, 33.89. Found: C, 17.61; H, 2.33; N, 34.11. Selected IR (KBr, cm^{-1}): 3,440(vs), 2,932(w), 1,663(vs), 1,434(s), 1,390(s), 1,255(w), 1,144(s), 1,101(m), 1,069(s), 952 (s), 772(w). ^1H NMR (400 MHz; D_2O) δ 7.75 (1H), 2.79 (3H), 2.67 (3H); ^{13}C NMR (400 MHz; D_2O) δ 165.9, 164.9, 67.8, 36.8, 31.3.

X-ray crystallographic analyses. Data were collected on an Oxford SuperNova (TM) CCD Diffractometer with a SuperNova X-ray Source (Mo-Kα). The structure was solved using SHELXS-97 and refined using SHELXL-97 contained in Olex2 programme. All hydrogen atoms were attached to their parent atom in a riding model, using the appropriate command. See Supplementary Data 1 and 2 for the CIF crystallographic information file, and Supplementary Methods for the discussion of data collection and refinement.

Characterization methods. Both compounds were characterized using a wide range of spectroscopy and other experimental techniques (such as powder X-ray diffraction, thermogravimetry analyses, ESI-MS, ICP, XPS, EPR, XANES). Details are provided. See Supplementary Methods for Material characterization.

Theoretical details. The theoretical analyses were performed to investigate the local symmetry of the cluster, the optimal spin multiplicity, oxidation state of Zn, effects of external R (Na, H, F and BrZn) ions on the structure of $[Zn_8(RL)_{12}]^{4-}$, MO analysis and nucleus-independent chemical shift indices, NBO and ELF analysis of the direct Zn–Zn bonding (see Supplementary Methods).

References

1. Lewis, G. N. The atom and the molecule. *J. Am. Chem. Soc.* **38,** 762–785 (1916).
2. Pauling, L. *The Nature of the Chemical Bond* 3rd edn, chapter 7 (Cornell Univ. Press, 1960).
3. Cotton, F. A., Murillo, C. A. & Walton, R. A. *Multiple Bonds Between Metal Atoms* 3rd edn (Springer, 2005).
4. Resa, I., Carmona, E., Gutierrez-Puebla, E. & Monge, A. Decamethyldizincocene, a stable compound of Zn(I) with a Zn-Zn bond. *Science* **305,** 1136–1138 (2004).
5. Hill, M. S., Hitchcock, P. B. & Pongtavornpinyo, R. A linear homocatenated compound containing six indium centers. *Science* **311,** 1904–1907 (2006).
6. Green, S. P., Jones, C. & Stasch, A. Stable magnesium(I) compounds with Mg-Mg bonds. *Science* **318,** 1754–1757 (2007).
7. Jones, C. *et al.* Amidinato- and guanidinato-cobalt(I) complexes: characterization of exceptionally short Co-Co interactions. *Angew. Chem. Int. Ed.* **48,** 7406–7410 (2009).
8. Zhu, Z. *et al.* Synthesis, structural characterization, and spectroscopy of the cadmium-cadmium bonded molecular species Ar'CdCdAr' (Ar' = C_6H_3-2,6-(C_6H_3-2,6-Pri_2)_2). *J. Am. Chem. Soc.* **128,** 15068–15069 (2006).
9. Nguyen, T. *et al.* Synthesis of a stable compound with fivefold bonding between two chromium(I) centers. *Science* **310,** 844–847 (2005).
10. Tsai, Y. C. *et al.* Journey from Mo-Mo quadruple bonds to quintuple bonds. *J. Am. Chem. Soc.* **131,** 12534–12535 (2009).
11. Li, T. S., Schulz, S. & Roesky, P. W. Synthesis, reactivity and applications of zinc-zinc bonded complexes. *Chem. Soc. Rev.* **41,** 3759–3771 (2012).
12. del Rio, D., Galindo, A., Resa, I. & Carmona, E. Theoretical and synthetic studies on $[Zn_2(\eta^5-C_5Me_5)_2]$: analysis of the Zn-Zn bonding interaction. *Angew. Chem. Int. Ed.* **44,** 1244–1247 (2005).
13. Carmona, E. & Galindo, A. Direct bonds between metal atoms: Zn, Cd, and Hg compounds with metal-metal bonds. *Angew. Chem. Int. Ed.* **47,** 6526–6536 (2008).
14. Grirrane, A. *et al.* Zinc-zinc bonded zincocene structures. synthesis and characterization of $Zn_2(\eta^5-C_5Me_5)_2$ and $Zn_2(\eta^5-C_5Me_4Et)_2$. *J. Am. Chem. Soc.* **129,** 693–703 (2006).
15. Bollermann, T. *et al.* The reactivity of $[Zn_2Cp^*_2]$: trapping monovalent {*ZnZnCp*} in the metal-rich compounds $[(Pd,Pt)(GaCp^*)_a(ZnCp^*)_{4-a}(ZnZnCp^*)_{4-a}]$ ($a = 0, 2$). *Angew. Chem. Int. Ed.* **50,** 772–776 (2011).
16. Wang, Y. *et al.* On the chemistry of Zn-Zn bonds, RZn-ZnR (R = [{(2,6-Pr$^i_2$C$_6$H$_3$)N(Me)C}$_2$CH]): synthesis, structure, and computations. *J. Am. Chem. Soc.* **127,** 11944–11945 (2005).
17. Zhu, Z. *et al.* Synthesis and characterization of the homologous M-M bonded series Ar'MMAr' (M = Zn, Cd, or Hg; Ar' = C_6H_3-2,6-(C_6H_3-2,6-Pr$^i_2$)_2) and related arylmetal halides and hydride species. *J. Am. Chem. Soc.* **129,** 10847–10857 (2007).
18. Schulz, S. *et al.* Structural characterization of a base-stabilized $[Zn_2]^{2+}$ cation. *Angew. Chem. Int. Ed.* **48,** 5748–5751 (2009).
19. del Rio, D. *et al.* IR and Raman characterization of the zincocenes (η^5-$C_5Me_5)_2Zn_2$ and (η^5-$C_5Me_5)(\eta^5$-$C_5Me_5)Zn$. *J. Phys. Chem. A* **112,** 10516–10525 (2008).
20. Nayek, H. P. *et al.* Aminotroponiminatozinc(I) complexes: syntheses and spectroscopic analyses. *Chem. Eur. J.* **17,** 1773–1777 (2011).
21. Lühl, A., Nayek, H. P., Blechert, S. & Roesky, P. W. Zinc-zinc bonded decamethyldizincocene $Zn_2(\eta^5-C_5Me_5)_2$ as catalyst for the inter- and intramolecular hydroamination reaction. *Chem. Commun.* **47,** 8280–8282 (2011).
22. Fedushkin, I. L. *et al.* [(dpp-bian)Zn-Zn(dpp-bian)]: a zinc-zinc-bonded compound supported by radical-anionic ligands. *Angew. Chem. Int. Ed.* **46,** 4302–4305 (2007).
23. Schnepf, A. & Himmel, H. J. Subvalent compounds featuring direct metal-metal bonds: the Zn-Zn bond in $[Cp^*_2Zn_2]$. *Angew. Chem. Int. Ed.* **44,** 3006–3008 (2005).
24. Li, X. *et al.* Observation of all-metal aromatic molecules. *Science* **291,** 859–861 (2001).
25. Boldyrev, A. I. & Wang, L. S. All-metal aromaticity and antiaromaticity. *Chem. Rev.* **105,** 3716–3757 (2005).
26. Kuznetsov, A. E. *et al.* All-metal antiaromatic molecule: rectangular Al_4^{4-} in the $Li_3Al_4^-$ anion. *Science* **300,** 622–625 (2003).
27. Kuznetsov, A. E., Corbett, J. D., Wang, L. S. & Boldyrev, A. I. Aromatic mercury clusters in ancient amalgams. *Angew Chem. Int. Ed.* **40,** 3369–3372 (2001).
28. Huang, X., Zhai, H. J., Kiran, B. & Wang, L. S. Observation of d-orbital aromaticity. *Angew. Chem. Int. Ed.* **44,** 7251–7254 (2005).
29. Zhai, H. J. *et al.* δ Aromaticity in $[Ta_3O_3]^-$. *Angew Chem. Int. Ed.* **46,** 4277–4280 (2007).
30. Galeev, T. R. & Boldyrev, A. I. Recent advances in aromaticity and antiaromaticity in transition-metal systems. *Annu. Rep. Prog. Chem. C: Phys. Chem.* **107,** 124–147 (2011).
31. Hirsch, A., Chen, Z. & Jiao, H. Spherical aromaticity in I_h symmetrical fullerenes: the $2(N + 1)^2$ rule. *Angew. Chem. Int. Ed.* **39,** 3915–3917 (2000).
32. Chen, X. M. & Tong, M. L. Solvothermal *in situ* metal/ligand reactions: a new bridge between coordination chemistry and organic synthetic chemistry. *Acc. Chem. Res.* **40,** 162–170 (2007).
33. Moulder, J. F., Stickle, W. F., Sobol, P. E. & Bomben, K. D. *Handbook of X-Ray Photoelectron Spectroscopy* 2nd edn (ed. Chastain, J.) (Perkin-Elmer Corporation, 1992).
34. Zubarev, D. Y., Averkiev, B. B., Zhai, H.- J., Wang, L.- S. & Boldyrev, A. I. Aromaticity and antiaromaticity in transition-metal systems. *Phys. Chem. Chem. Phys.* **10,** 257–267 (2008).
35. Benson, F. R. The chemistry of the tetrazoles. *Chem. Rev.* **41,** 1–61 (1947).

Author contributions

P.C. and H.-S.H. performed the experimental work and theoretical study, respectively, and contributed equally to this work. J.T.M. conducted the X-ray absorption spectroscopy and interpretation of the results. P. C. analysed the EPR and magnetic properties. B.Z. and J.L. designed, directed and supervised the project. All authors contributed to analysing the data and discussing the results. P.C., H.-S.H., B.Z. and J.L. co-wrote the paper.

Additional information

Accession codes: The X-ray crystallographic coordinates for structures reported in this Article have been deposited at the Cambridge Crystallographic Data Centre (CCDC), under deposition number CCDC 879470 for **1** and 879472 for **2**. These data can be obtained free of charge from The Cambridge Crystallographic Data Centre via www.ccdc.cam.ac.uk/data_request/cif.

Supplementary Information accompanies this paper at http://www.nature.com/naturecommunications.

Competing financial interests: The authors declare no competing financial interests.

Reprints and permission information is available online at http://npg.nature.com/reprintsandpermissions.

How to cite this article: Cui, P. *et al.* A multicentre-bonded $[Zn^I]_8$ cluster with cubic aromaticity. *Nat. Commun.* 6:6331 doi: 10.1038/ncomms7331 (2015).